Resonances in the optical response of a slab with time-periodic dielectric function $\epsilon(t)$

Jorge R. Zurita-Sánchez and P. Halevi
Instituto Nacional de Astrofísica, Óptica y Electrónica, Apartado Postal 51, Puebla, Pue. 72000, Mexico
(Received 17 December 2009; published 19 May 2010)

We demonstrate that the optical response of a periodically modulated dynamic slab exhibits infinite resonances for frequencies $\omega = (\Omega/2)(2l+1)$, namely, odd multiples of one-half of the modulating frequency Ω of the dielectric function $\epsilon(t)$. These frequencies coincide partially with the usual condition of parametric amplification. However, the resonances occur only for certain normalized slab thicknesses L_R. These resonances follow from detailed numerical studies based on our recent paper [Zurita-Sánchez, Halevi, and Cervantes-González, Phys. Rev. A **79**, 053821 (2009)]. As the thickness L nearly matches a resonance thickness L_R, the amplitudes of counterpropagating modes in the slab obey a condition implying that both have the same modulus and their phases match a condition related to L_R and the bulk wave vectors. When this condition is met, the electric field profile inside the slab is a superposition of standing waves with odd and even symmetries, and the reflection and transmission coefficients can reach great values and become infinite at exact resonance. Numerical simulations of the optical response are shown for a sinusoidal $\epsilon(t)$ with either moderate or strong modulation. As expected, as the modulation strength increases, higher-order harmonics $\omega - n\Omega$ ($n = 0, \pm 1, \pm 2, \ldots$) become more noticeable, and short-wavelength bulk modes contribute significantly. However, we found that, regardless of the excitation frequency $\omega = (\Omega/2)(2l+1)$, the dominant spectral component of the generated fields is $\Omega/2$. Also, as the excitation frequency increases, the parity of the standing waves is conserved.

DOI: 10.1103/PhysRevA.81.053834 PACS number(s): 42.25.Bs

I. INTRODUCTION

In a previous paper [1], we developed a general theory of the electromagnetic response of a monochromatic wave incident at a dynamic slab with a time-periodic dielectric function $\epsilon(t) = \epsilon(t+T)$ (T being the period). As a consequence of the modulation of $\epsilon(t)$ that is realized by an (unspecified) external agent, the reflected and transmitted fields result in a superposition of waves with harmonics $\omega_0 - \Omega n$ (ω_0 is the excitation frequency, $\Omega \equiv 2\pi/T$, and $n = 0, \pm 1, \pm 2, \ldots$). In this paper, we apply the aforementioned theory to frequencies of incidence ω_0 that are odd multiples of $\Omega/2$. This condition requires special attention because $\omega_0 = l\Omega/2$ (l being an odd integer) corresponds to odd frequencies of parametric excitation. Our system is driven by an external source (the incident wave), and the slab thickness is an important parameter. Our aim is to study the conditions for and features of resonant amplification of an electromagnetic wave when incident at a periodically modulated dynamic slab.

Pioneering studies with time-dependent $\epsilon(t)$ date back about half a century, as reviewed in Ref. [1]. In particular, it was noted that dynamic media could have engineering applications as amplifiers [2]. However, the first theoretical analysis of such amplification in a periodically modulated dynamic slab was realized by Holberg and Kunz [3]. These authors restricted themselves to the case of a specific variation $\epsilon(t)$ that gives rise to Mathieu functions for the field, and to a weakly modulated slab.

On the other hand, an effect closely related to ours is the resonant response for photon generation from vacuum in a cavity when the mirrors oscillate at a frequency that is twice an eigenfrequency of the unperturbed cavity (dynamic Casimir effect); see, for example, Ref. [4]. Finally, we mention that interaction of electromagnetic fields with dynamic media has recently become an active topic of research, and applications for controlling energy transport are promising (see Ref. [1] and references therein). We supplement the list of references contained in our previous work [1] with the following recent studies. In Ref. [5], a theory of radiation produced by currents embedded in time-varying media is presented. The coupling between modes of a cavity is achieved by the temporal change of the refractive index [6,7].

Next we present the organization of the paper. In Sec. II, we recapitulate the essential aspects of our theory in Ref. [1]. Section III states the conditions for the occurrence of resonances in a dynamic slab. Numerical simulations for particular cases are described in Sec. IV. The first part analyzes the transmitted field; the second part deals in detail with the approach to a resonance (the Appendix complements this part); and the third part concerns the field profiles inside the slab. Finally, the conclusions are presented in Sec. V.

II. RECAPITULATION OF THEORY

A slab occupies the region $0 < y < L$ and has a time-periodic dielectric function [$\epsilon(t) = \epsilon(t+T)$, T being the period]. The medium outside the slab is vacuum ($\epsilon = 1$). We assume that a plane wave coming from $y < -\infty$, with angular frequency ω_0, is incident normally at the surface $y = 0$. Without loss of generality, the electric (magnetic) field has only a z (x) component.

The electric field of the incident wave is

$$E_{\rm inc}(y,t) = E_0 e^{i[k_0(\omega_0)y - \omega_0 t]}. \tag{1}$$

Here, $k_0(\omega_0) \equiv \omega_0/c$ (c being the velocity of light) and E_0 is the amplitude of the plane wave. The reflected and transmitted electric fields are superpositions of waves with the frequency harmonics $\omega_0 - n\Omega$ generated in the dynamic slab, that is,

$$E_r(y,t) = \sum_{n=-\infty}^{\infty} E_n^r e^{-i[k_n(\omega_0)y + (\omega_0 - \Omega n)t]}, \tag{2}$$

$$E_t(y,t) = \sum_{n=-\infty}^{\infty} E_n^t e^{i[k_n(\omega_0)(y-L)-(\omega_0-\Omega n)t]}. \quad (3)$$

Here $k_n(\omega_0) = (\omega_0 - \Omega n)/c$ is the wave vector for each of the reflected (transmitted) harmonics. The electric field $E_{\text{slab}}(y,t)$ inside the slab is

$$E_{\text{slab}}(y,t) = \sum_{n=-\infty}^{\infty} E_n^s(y) e^{-i(\omega_0-n\Omega)t}, \quad (4)$$

where

$$E_n^s(y) = \sum_{p=1}^{\infty} (A_p e^{ik_p(\omega_0)y} + B_p e^{-ik_p(\omega_0)y}) e_{pn}(\omega_0). \quad (5)$$

This field is a superposition of p modes of the corresponding bulk dynamic medium that propagate in the left and right directions. Each (bulk) p mode is given by the sum of partial harmonics n with amplitude $e_{pn}(\omega_0)$, wave vector $k_p(\omega_0)$, and frequency $\omega_0 - n\Omega$. Of course, $A_p e_{pn}(\omega_0)$ $[B_p e_{pn}(\omega_0)]$ is the amplitude of a plane wave propagating in the slab to the right [left] with wave vector $k_p(\omega_o)$ and frequency $\omega_0 - n\Omega$.

The coefficients E_n^r, E_n^t, A_p, and B_p are obtained by solving the linear system

$$E_0\delta_{n0} + E_n^r = \sum_p e_{pn}(\omega_0)(A_p + B_p), \quad (6)$$

$$E_0\delta_{n0} - E_n^r = \sum_p \frac{e_{pn}(\omega_0)k_p(\omega_0)c}{\omega_0 - n\Omega}(A_p - B_p), \quad (7)$$

$$E_n^t = \sum_p e_{pn}(\omega_0)(A_p e^{ik_p(\omega_0)L} + B_p e^{-ik_p(\omega_0)L}), \quad (8)$$

$$E_n^t = \sum_p \frac{e_{pn}(\omega_0)k_p(\omega_0)c}{\omega_0 - n\Omega}(A_p e^{ik_p(\omega_0)L} - B_p e^{-ik_p(\omega_0)L}). \quad (9)$$

This linear system arises from the boundary conditions that the electromagnetic fields must satisfy at the interfaces $y = 0$ and L. These equations are valid if ω_0/Ω is *not* an integer. This condition is obeyed in the present paper.

III. RESONANCES

Performing numerical simulations beyond those reported in Ref. [1], we have found that the amplitudes of the reflected and transmitted harmonics can be many orders of magnitude larger than the amplitude of the incoming wave. Next we discuss under what circumstances this happens.

We have encountered that a necessary condition for this effect to occur is that the frequency of the incident wave be

$$\omega_0 = \Omega(2l+1)/2, \qquad l = 0,1,2,\ldots \quad (10)$$

These frequencies coincide with the odd resonant frequencies of parametric amplification; see, for example, Ref. [8]. However, this condition is not sufficient. In addition, these resonances are realized only for certain slab thicknesses (geometric condition). Importantly, the large amplifications of the reflected and transmitted fields appear for thicknesses L lying in quite a small interval around certain resonant thicknesses L_R for which, presumably, the stability of the dynamic system is broken owing to the divergence of the fields.

Within an extremely small interval centered at a resonant thickness L_R, we find numerically that

$$B_p \approx \pm A_p e^{ik_p L}. \quad (11)$$

The condition (11) implies that (i) the magnitudes of the amplitudes A_p and B_p [see Eq. (5)] are almost equal, namely,

$$|A_p| \approx |B_p| \equiv D_p, \quad (12)$$

and (ii) the phases of A_p and B_p, $\phi_p^{A(B)} = \text{Arg}[A(B)_p]$ $(-\pi < \phi_p^{A(B)} \leqslant \pi)$, satisfy

$$\phi_p^B - \phi_p^A \approx k_p L - m_p\pi, \quad p = 1,2,\ldots, \quad (13)$$

where m_p is an integer. We have restricted the range to $-\pi < \phi_p^{A(B)} \leqslant \pi$ only for convenience in the following numerical analysis.

Using the conditions (12) and (13) in Eq. (5), the electric field distribution inside the slab becomes

$$E_n^s(y) = \sum_{p=1}^{\infty} 2D_p e^{i(k_p L/2+\phi_p^A)} e_{pn}(\omega_0) \times \begin{cases} \cos[k_p(y-L/2)], & m_p \text{ even}, \\ i\sin[k_p(y-L/2)], & m_p \text{ odd}. \end{cases} \quad (14)$$

By substituting Eq. (14) into Eq. (4), we can see that the spatial and temporal oscillations of $\text{Re}[E_{\text{slab}}(y,t)]$ have become independent of each other. That is, the field distribution $E_n^s(y)$ [Eq. (14)] describes a superposition of *stationary waves*. Moreover, this distribution exhibits a simple even or odd symmetry with respect to the center of the slab ($y = L/2$).

The frequencies $\Omega(2l+1)/2$ ($l = 0,1,2,\ldots$) are the borders of the temporal Brillouin zones. For these frequencies, the wave vectors k_p (p being a positive integer) are either the lower or the upper limits of a forbidden wave-vector band gap. When the frequency ω_0 is set to such a Brillouin zone edge, a strong mixing of modes takes place, resulting in the forbidden k band gaps. However, "pure" stationary waves are obtained when the amplitudes A_p and B_p satisfy condition (11).

In the next section, we will demonstrate numerically that the conditions (10) and (11) indeed lead to resonant amplification of the reflection and transmission amplitudes.

IV. NUMERICAL SIMULATIONS

We consider that the dielectric function is modulated sinusoidally as

$$\epsilon(t) = \epsilon_0 + \Delta\epsilon\sin(\Omega t), \quad (15)$$

where $\Omega = 2\pi/T$. For a consistent comparison with our previous work, the values for ϵ_0 and $\Delta\epsilon$ are the same that were chosen in Ref. [1]. Hereafter $\epsilon_0 = 5.25$, while $\Delta\epsilon = 0.85$ (moderate modulation) or $\Delta\epsilon = 3.4$ (strong modulation). We have solved Eqs. (6)–(9) for the transmission coefficients E_n^t (Sec. IV A below) and for the amplitudes A_p and B_p that lead to the electric field profiles in the slab (Sec. IV C).

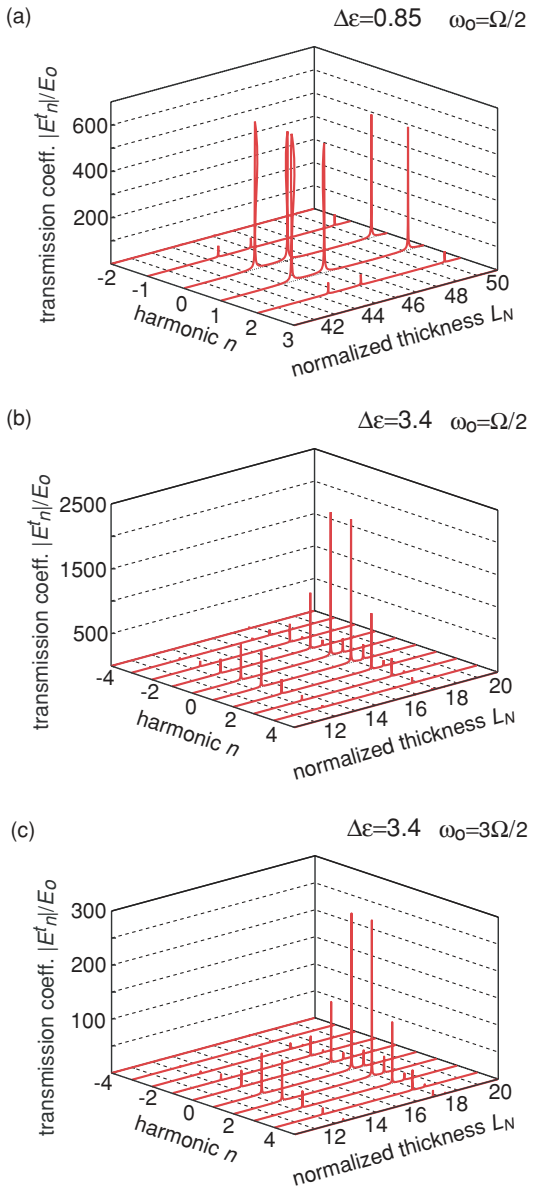

FIG. 1. (Color online) Transmission coefficients E_n^t as functions of the normalized thickness L_N. (a) $\omega_0 = \Omega/2$, $\Delta\epsilon = 0.85$ (moderate modulation), and $n = -2,-1,\ldots,3$. (b) $\omega_0 = \Omega/2$, $\Delta\epsilon = 3.4$ (strong modulation), and $n = -4,-3,\ldots,5$. (c) $\omega_0 = 3\Omega/2$, $\Delta\epsilon = 3.4$ (strong modulation), and $n = -4,-3,\ldots,5$.

A. Transmission

We consider the case $\omega_0 = \Omega/2$. In Figs. 1(a) and 1(b), we plot the magnitudes of the transmission coefficients E_n^t/E_0 for the first harmonics as functions of the normalized slab thickness,

$$L_N = L\sqrt{\epsilon_0}\Omega/c, \tag{16}$$

for $\Delta\epsilon = 0.85$ and 3.4. These figures show that resonances arise for certain slab thicknesses. For the moderate-modulation case, the resonances (beyond 40) show up for $L_N \approx 43.48, 45.08, 49.20$ [see Fig. 1(a)], while for the strong-modulation case (beyond 10) they appear for $L_N \approx 12.38, 16.79, 17.39$ [see Fig. 1(b)]. As a consequence, as the modulation strength $\Delta\epsilon$ increases, the first resonance occurs for a smaller normalized thickness L_N. Also, we notice that higher-order harmonics become more appreciable as the strength $\Delta\epsilon$ increases. At a resonance, for both cases, the largest (and equal) magnitudes of the transmission coefficients E_n^t/E_0 correspond to the harmonics $n = 0,1$. These harmonics both oscillate with the frequency $|\omega_0 - n\Omega| = \Omega/2$. In the limit of the empty-lattice model, the dispersion curves corresponding to branches $n = 0,1$ intersect at the frequency $\Omega/2$. Consequently, a strong coupling between these equally important harmonics $n = 0,1$ must take place.

The magnitudes of the transmission coefficients E_n^t/E_0 for the first harmonics as functions of the normalized slab thickness L_N for $\omega_0 = 3\Omega/2$ and $\Delta\epsilon = 3.4$ (strong modulation) are depicted in Fig. 1(c). From the comparison of Figs. 1(b) and 1(c), we recognize that the resonances for both cases occur at the same thicknesses. However, the magnitude of the transmission coefficient E_n^t/E_0 is about one order of magnitude larger for $\omega_0 = \Omega/2$ than for $\omega_0 = 3\Omega/2$. Consequently, the magnitudes of the transmission coefficients E_n^t/E_0 decrease as the number l in Eq. (10) increases. Differently from the case $\omega_0 = \Omega/2$, for $\omega_0 = 3\Omega/2$ the largest amplitudes of the transmission coefficients E_n^t/E_0 correspond to the harmonics $n = 1,2$. In the empty-lattice limit, the dispersion branches $n = 1,2$ cross each other at the frequency $3\Omega/2$. This explains that the harmonics $n = 1,2$ are strongly coupled. These harmonics actually oscillate with frequency $|\omega_0 - n\Omega| = \Omega/2$. Thus, the dominant spectral component generated at resonance is the one with frequency $\Omega/2$, regardless of the frequency of incidence ω_0 (odd multiples of $\Omega/2$).

We have mentioned that transmission coefficients E_n^t/E_0 around a resonance thickness can be very large. In addition, they change abruptly as the thickness is slightly modified. To illustrate this, let us consider the normalized thickness $L_N = 45.084\,113\,79$ for the case of Fig. 1(a). If this L_N is rounded to six decimal places (45.084 114) then the transmission coefficients E_n^t/E_0 will be reduced by about two orders of magnitude. For practical reasons arising from this fact, the "sampling" step used in the plots of Fig. 1 is not small enough to show a still larger amplification of the fields.

Next we take a closer look at the particular thickness $L_N = 45.084\,113\,79$ ($L_N = 16.788\,791\,99$) for the moderate-(strong-)modulation case. The transmission coefficients E_n^t/E_0 for the first harmonics at an excitation frequency $\omega_0 = \Omega/2$ are plotted in Figs. 2(a) and 2(b). These figures show that the magnitudes of the transmission coefficients E_n^t/E_0 can reach very large values ($\sim 10^8$). We remark that the modulating external agent of the dynamic slab apparently provides the energy to amplify the transmitted (and reflected) field. We already pointed out that, as the modulation strength $\Delta\epsilon$ increases, higher harmonics become more noticeable. Also, Figs. 2(a) and 2(b) display clearly the aforementioned feature that the harmonics $n = 0,1$ have the largest transmission coefficient magnitudes.

Now we consider the case $L_N = 16.788\,791\,99$ and strong modulation, but the exciting frequency is increased to $\omega_0 = 3\Omega/2$. The magnitudes of the the transmission coefficients E_n^t/E_0 for the generated harmonics are plotted in Fig. 2(c). The comparison of Figs. 2(b) and 2(c) shows that the magnitudes of the transmission coefficients E_n^t/E_0 for $\omega_0 = \Omega/2$ are larger

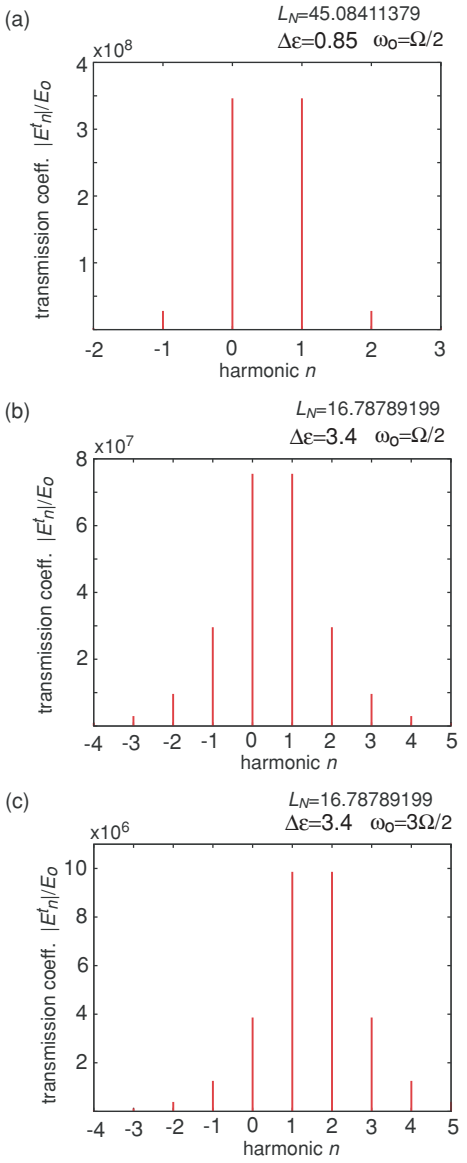

FIG. 2. (Color online) Transmission coefficients E_n^t for various harmonics n at a resonance thickness. (a) $\omega_0 = \Omega/2$, $\Delta\epsilon = 0.85$ (moderate modulation), $n = -2,-1,\ldots,3$, and $L_N = 45.084\,113\,79$ (b) $\omega_0 = \Omega/2$, $\Delta\epsilon = 3.4$ (strong modulation), $n = -4,-3,\ldots,5$, and $L_N = 16.788\,791\,99$. (c) $\omega_0 = 3\Omega/2$, $\Delta\epsilon = 3.4$ (strong modulation), $n = -4,-3,\ldots,5$, and $L_N = 16.788\,791\,99$.

than those for $\omega_0 = 3\Omega/2$. Again, as was also noted from comparison of Figs. 1(b) and 1(c), it is evident from Fig. 2(c) that the dominant spectral contributions to the transmitted field arise from the harmonics $n = 1,2$, which both oscillate at the frequency $\Omega/2$.

The magnitudes of the reflection coefficients E_n^r/E_0 are the same as the magnitudes of the transmission coefficients E_n^t/E_0 when the thickness L almost coincides with a resonant thickness. Hence, we have omitted the analysis for the reflected field.

We note that in Figs. 1 and 2 the transmission resonances always appear as pairs of harmonics (n_1,n_2), such that $|E_{n_1}^t| = |E_{n_2}^t|$. Not surprisingly, the values n_1,n_2 correspond to equal frequencies $|\omega_0 - n_1\Omega| = |\omega_0 - n_2\Omega|$. With the help of Eq. (10), we readily find that $n_1 + n_2 = 2n + 1$. Clearly, this is satisfied for all the examples in Figs. 1 and 2.

B. A detailed look at a resonance

Previously, we have mentioned that the stability of the dynamic system is presumably broken at the resonant thickness L_R. Now we examine a resonance numerically.

We solve the linear system Eqs. (6)–(9) by using the single-value decomposition method [9]. In addition to finding the solution, this method allows us to estimate how singular is the coefficient matrix $\mathbb{A}$ of our linear system [see Eqs. (6)–(9)]. More about this estimation is found in the Appendix. We consider that $\mathbb{A}$ is a square matrix of order M. We choose the case $\Delta\epsilon = 3.4$ (strong modulation) and $\omega_0 = \Omega/2$. In Fig. 3, we plot the coefficient D_1/E_0 [see Eq. (12)] as a function of the normalized thickness L_N near a resonance for the matrices $\mathbb{A}$ of order $M = 188$, 228, 268, and 284. In this plot, the thickness interval is $a < L_N < a + 5\times10^{-10}$ ($a = 16.788\,792\,025\,2$). We note from Fig. 3 that D_1/E_0 increases by about three orders of magnitude in this tiny interval. The peak shape looks like a legitimate resonance. However, the peaks shown have finite heights and slightly different shapes depending on the matrix order M. Unexpectedly, the peak height turns out to be the largest (smallest) for the smallest (second largest) matrix order $M = 188$ ($M = 268$). We attribute these features to numerical artifacts that are discussed in the Appendix. Thus, according to the numerical analysis in the aforementioned Appendix, the resonance of the dynamic slab can be considered indeed legitimate, namely, as $L \to L_R$, the magnitude of the reflection and transmission coefficients $|E_n^{r,t}|/E_0 \to \infty$.

As we pointed out in our previous work [1], we are dealing with an open system. Hence, the energy balance between the energy of the incident wave and the energy of the reflected and transmitted waves is not necessarily conserved. The energy gained is provided by the external agent that modulates the dynamic medium. For a nonideal situation, the amplification enhancement should be limited by the amount of energy that this external agent can supply and the absorption of the dynamic medium (herein neglected).

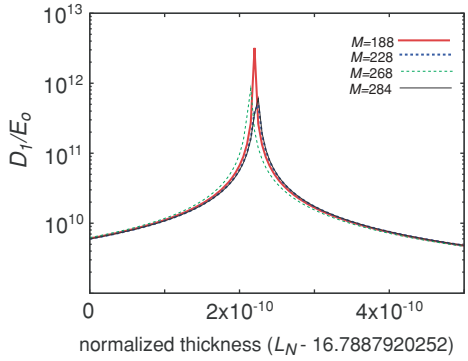

FIG. 3. (Color online) Amplitude coefficient D_1/E_0 as a function of the normalized thickness L_N near a resonance for $\Delta\epsilon = 3.4$, $\omega_0 = \Omega/2$, and the coefficient matrices $\mathbb{A}$ of orders $M = 188,228,268,284$.

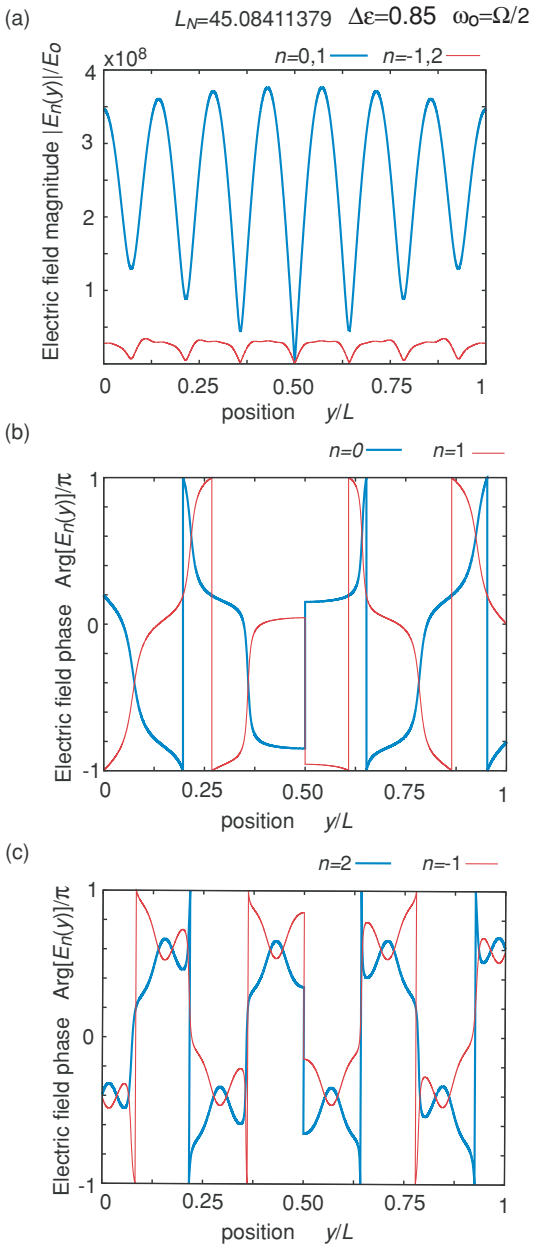

FIG. 4. (Color online) Electric field profiles in the slab for $L_N = 45.084\,113\,79$, $\Delta\epsilon = 0.85$ (moderate modulation), and $\omega_0 = \Omega/2$. (a) Magnitudes of the electric field $E_n^s(y)$ for harmonics $n = -1,0,1,2$. (b) Phases of the electric field $E_n^s(y)$ for harmonics $n = 0,1$. (c) Phases of the electric field $E_n^s(y)$ for harmonics $n = -1,2$.

C. Electric field profiles in the slab

We stated in Sec. III that a superposition of standing waves [see Eq. (14)] is created inside the slab when the resonance conditions (10) and (11) are met. Next we illustrate these standing waves.

First, we consider the case $\Delta\epsilon = 0.85$ (moderate modulation), $L_N = 45.084\,113\,79$, and $\omega_0 = \Omega/2$. The magnitudes of the electric field $E_n^s(y)$ for the harmonics $n = -1,0,1,2$ are plotted in Fig. 4(a). As can be seen, the electric field distributions inside the slab are the same for the harmonics $n = 0,1$ and for the harmonics $n = -1,2$. The former pair of harmonics oscillate with frequency $\Omega/2$, while the latter oscillate with frequency $3\Omega/2$. We note that the magnitudes of the electric field $E_n^s(y)$ for the harmonics $n = 0,1$ are about an order of magnitude larger than those for the harmonics $n = -1,2$. Thus, the total electric field $E_{\rm slab}(y,t)$ for the moderate-modulation case is composed predominantly of the electric field distribution of the harmonics $n = 0,1$. Also, we can recognize that the parity of the standing-wave pattern is odd since the electric field $E_n^s(y)$ vanishes at the center of the slab ($y = L/2$) [see Eq. (14)]. The phases of the electric field $E_n^s(y)$ for the harmonics $n = -1,0,1,2$ are shown in Figs. 4(b) and 4(c). As seen in Figs. 4(b) and 4(c), there are phase discontinuities at the center of the slab since the electric field vanishes there. For odd parity, the phases of the electric field $E_n^s(y)$ for the harmonics m,n ($m + n =$ odd integer) that oscillate with the same frequency are related to each other by

$$\mathrm{Arg}\left[E_n^s(y - L/2)/E_0\right] + \mathrm{Arg}\left[E_m^s(-\{y - L/2\})/E_0\right] = a, \tag{17}$$

where a is a constant. This relation is illustrated in Figs. 4(b) [4(c)], where the harmonics $n = 0$ and $m = 1$ [$n = -1$ and $m = 2$] oscillate with frequency $\Omega/2$ [$3\Omega/2$]. The electric field profile $E_n^s(y)$ is a superposition of p modes [see Eq. (14)]. The amplitudes D_p of the modes for $p = 1,\ldots,5$ are tabulated in Table I. As seen, for $p = 1$ and 2 these amplitudes are at least two orders of magnitude greater than the others. Also, Table I lists the normalized wave vectors κ_p, the phases $\phi_p^{A,B}/\pi$, and m_p. These quantities corroborate the condition (13). The numbers m_p are odd integers, in agreement with the odd symmetry of the profiles E_n^s that we discussed.

Next we analyze the case in which the slab is strongly modulated ($\Delta\epsilon = 3.4$, $L_N = 16.788\,791\,99$] and excited with frequency $\omega_0 = \Omega/2$. The magnitudes of the electric field $E_n^s(y)$ inside the slab for the harmonics $n = -1,0,1,2$ are plotted in Fig. 5(a). As for the moderate modulation, the pair of harmonics that oscillate with the same frequency have the same magnitude. In contrast to the previous case, the electric field does not vanish at the center of the slab. Therefore the parity corresponding to this resonance is *even* [see Eq. (14)]. For any position y, the magnitude of the electric field $E_n^s(y)$ for the harmonics $n = 0,1$ ($\Omega/2$) is considerably larger than for the other harmonics. This also happens for the moderate-modulation case. However, now the total electric field $E_{\rm slab}(y,t)$ is not due mainly to the harmonics $n = 0,1$, but higher-order harmonics must be also taken into account. Figures 5(b) and 5(c) show the phases of the electric field $E_n^s(y)$ for the harmonics $n = -1,0,1,2$. We notice that the

TABLE I. $\kappa_p \equiv k_p c/(\sqrt{\epsilon_0}\Omega)$, D_p, $\phi_p^{A,B}/\pi$, and m_p for $p = 1,\ldots,5$, $\omega_0 = \Omega/2$, $L_N = 45.084\,113\,79$, and $\Delta\epsilon = 0.85$ (moderate modulation).

p	κ_p	D_p	ϕ_p^A/π	ϕ_p^B/π	m_p
1	0.477 41	1.5789×10^8	0.922 17	0.773 41	7
2	0.518 04	1.0277×10^8	−0.369 32	0.064 90	7
3	1.492 86	5.4806×10^6	0.635 97	−0.940 39	23
4	1.492 87	3.4656×10^6	−0.364 12	0.059 70	21
5	2.487 77	1.2554×10^5	−0.002 84	0.698 42	35

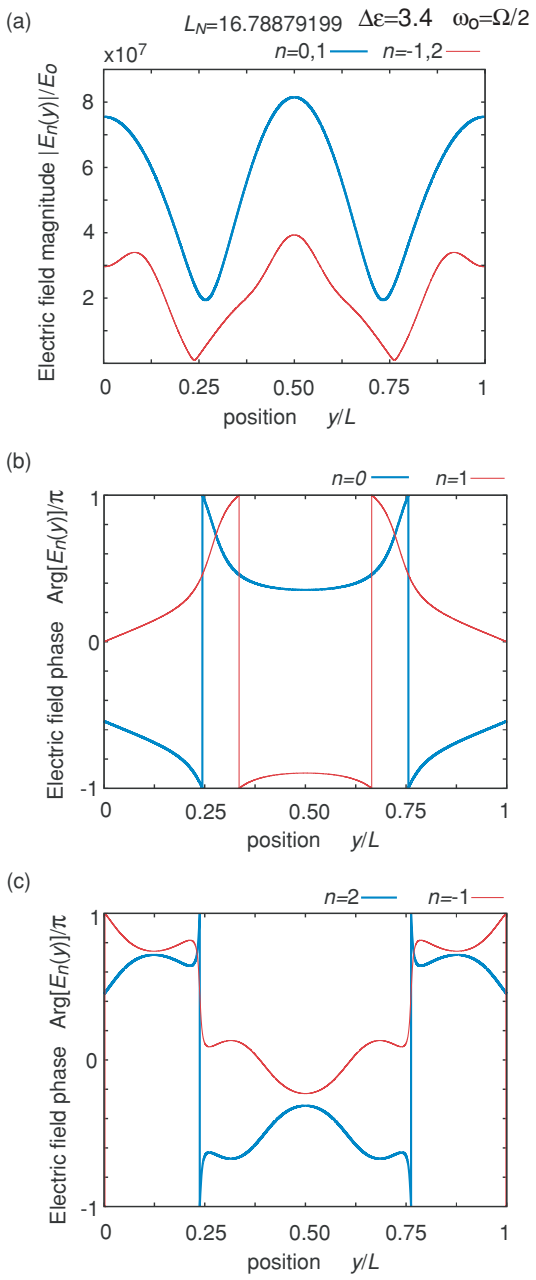

FIG. 5. (Color online) Electric field profiles in the slab for $L_N = 16.788\,791\,99$, $\Delta\epsilon = 3.4$ (strong modulation), and $\omega_0 = \Omega/2$. (a) Magnitudes of the electric field $E_n^s(y)$ for harmonics $n = -0,1,2,3$. (b) Phases of the electric field $E_n^s(y)$ for harmonics $n = 1,2$. (c) Phases of the electric field $E_n^s(y)$ for harmonics $n = 0,3$.

phase for a given harmonic n is an even function with respect to the center of the slab $y = L/2$. Furthermore,

$$\mathrm{Arg}\left[E_n^s(y - L/2)/E_0\right] + \mathrm{Arg}\left[E_m^s(y - L/2)/E_0\right] = b, \quad (18)$$

where b is a constant, and m,n ($m + n =$ odd integer) correspond to the harmonics that oscillate at the same frequency. Table II shows the values of D_p for $p = 1,\ldots,7$. Similarly to what was seen for the moderate-modulation case, the largest D_p's correspond to $p = 1$ and 2. However, while for the moderate-modulation case D_p for $p = 5$ is reduced by about

TABLE II. $\kappa_p \equiv k_p c/(\sqrt{\epsilon_0}\Omega)$, D_p, $\phi_p^{A,B}/\pi$, and m_p for $p = 1,\ldots,7$, $\omega_0 = \Omega/2$, $L_N = 16.788\,791\,99$, and $\Delta\epsilon = 3.4$ (strong modulation).

p	κ_p	D_p	ϕ_p^A/π	ϕ_p^B/π	m_p
1	0.370 08	3.7687×10^7	−0.509 62	−0.531 92	2
2	0.543 73	1.5875×10^7	0.526 38	−0.567 92	4
3	1.363 87	8.1281×10^5	0.334 95	−0.376 49	8
4	1.365 03	4.9039×10^6	0.331 84	−0.373 38	8
5	2.267 12	6.4821×10^5	−0.578 57	−0.462 97	12
6	2.267 13	6.1100×10^5	−0.078 59	0.037 06	12
7	3.171 54	3.9146×10^4	0.504 77	−0.546 38	18

three orders of magnitude with respect to the largest D_p, the same reduction level for the strong-modulation case is reached for $p = 7$. Thus, as the modulation strength $\Delta\epsilon$ increases, more p modes contribute to the electric field $E_n^s(y)$. In addition, Table II contains the values of m_p ($p = 1,\ldots,7$). As seen, all m_p are even numbers, which confirms the even parity of $E_n^s(y)$. Table II comprises the values of the normalized κ_p and $\phi_p^{A,B}/\pi$ for $p = 1,\ldots,7$; thus condition (13) can be verified.

Now we set the excitation frequency to $\omega_0 = 3\Omega/2$, while still dealing with the strong-modulation case ($\Delta\epsilon = 3.4$, $L_N = 16.788\,791\,99$). We plot the magnitudes of the electric field $E_n^s(y)$ for the harmonics $n = 0,1,2,3$ in Fig. 6(a). Again, the magnitudes of the electric field $E_n^s(y)$ for the harmonics oscillating at the same frequency are equal and are greatest for the harmonics oscillating with frequency $\Omega/2$, that is, $n = 1,2$. A comparison of Figs. 5(a) and 6(a) shows that they look very similar. However, the field magnitudes in Fig. 5(a) are one order of magnitude larger than those in Fig. 6(a). As we pointed out, the amplification is stronger for $\omega_0 = \Omega/2$ than for $\omega_0 = 3\Omega/2$. The corresponding phases of the electric field $E_n^s(y)$ for the harmonics $n = 0,1,2,3$ are plotted in Figs. 6(b) and 6(c). We observe that the even parity is maintained, as for the $\omega_0 = \Omega/2$ case. In addition, the curves in Figs. 6(b) and 6(c) are mirror plots of those in Figs. 5(b) and 5(c) with respect to the y axis. The values of D_p and m_p for $p = 1,\ldots,7$ appear in Table III. As expected, the magnitudes D_p for the excitation frequency $\omega_0 = 3\Omega/2$ are smaller than those for $\omega_0 = \Omega/2$ (see Tables II and III). As in Table II, the values of m_p are all even. This shows that the parity of E_n^s is conserved as the excitation frequency increases from $\omega_0 = \Omega/2$ to $3\Omega/2$.

TABLE III. $\kappa_p \equiv k_p c/(\sqrt{\epsilon_0}\Omega)$, D_p, $\phi_p^{A,B}/\pi$, and m_p for $p = 1,\ldots,7$, $\omega_0 = 3\Omega/2$, $L_N = 16.788\,791\,99$, and $\Delta\epsilon = 3.4$ (strong modulation).

p	κ_p	D_p	ϕ_p^A/π	ϕ_p^B/π	m_p
1	0.370 08	4.9222×10^6	0.539 58	0.517 29	2
2	0.543 73	2.0735×10^6	−0.924 41	−0.018 72	2
3	1.363 87	1.0616×10^5	0.384 16	−0.327 29	8
4	1.365 03	6.4050×10^5	0.381 04	−0.324 17	8
5	2.267 12	8.4663×10^4	0.470 64	0.586 23	12
6	2.267 13	7.9802×10^4	0.470 61	0.586 26	12
7	3.171 54	5.1128×10^3	0.554 05	−0.497 11	18

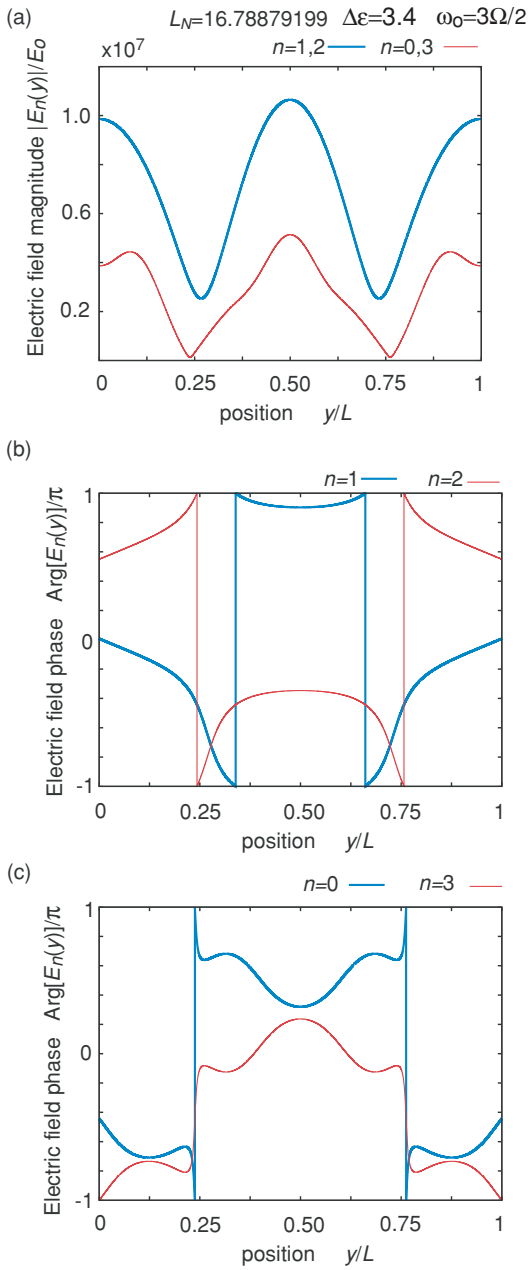

FIG. 6. (Color online) Electric field profiles in the slab for $L_N = 16.788\,791\,99$, $\Delta\epsilon = 3.4$ (strong modulation), and $\omega_0 = 3\Omega/2$. (a) Magnitudes of the electric field $E_n^s(y)$ for harmonics $n = -0,1,2,3$. (b) Phases of the electric field $E_n^s(y)$ for harmonics $n = 1,2$. (c) Phases of the electric field $E_n^s(y)$ for harmonics $n = 0,3$.

Again, the condition (13) can be verified for $p = 1,\ldots,7$, the values of normalized κ_p and $\phi_p^{A,B}/\pi$ being listed in Table III.

The transmission and reflection coefficients can be related to the electric field at the surfaces of the slab ($y = 0$ and L) as

$$E_n^r = E_n^s(0) - E_0\delta_{n0}, \tag{19}$$

$$E_n^t = E_n^s(L). \tag{20}$$

Equations (19) and (20) follow straightforwardly by comparing Eq. (5) with Eqs. (6) and (8). From the field profiles given by Eq. (14), it turns out that $E_n^s(0) = E_n^s(L)$ for even parity, whereas $E_n^s(0) = -E_n^s(L)$ for odd parity. Consequently, *the magnitudes of* E_n^t and E_n^r *are the same for* $n \neq 0$. Moreover, if $|E_0^s(0)| \gg |E_0|$ then the last statement is even valid approximately for $n = 0$. This justifies our omission of analysis for the reflected field. Also, Eq. (20) can be verified by looking at Figs. 2–6.

V. CONCLUSIONS

We have shown that huge resonant amplification of an incident wave can be achieved in a periodically modulated dynamic slab surrounded by vacuum. As seen from Fig. 2(a), transmission amplitudes on the order of 10^8 can be achieved for slab thicknesses in the immediate vicinity of a resonant value L_R. This amplification happens for excitation frequencies equal to odd multiples of one-half the modulation frequency Ω, provided that the condition (11) is satisfied. When this condition is met, the electric field profile inside the slab is a superposition of standing waves with odd and even symmetries. We have considered that $\epsilon(t)$ oscillates sinusoidally with either strong or moderate modulation and have performed numerical simulations for these cases. An important point is that we have realized a numerical analysis near a resonance and found that the resonances of a dynamic slab are indeed legitimate, namely, the fields become infinite as the thickness L approaches a resonant thickness L_R. In addition, the numerical outcomes reveal the following behavior. The transmission coefficient E_n^t/E_0 around a resonant thickness varies extremely rapidly as the thickness is slightly modified. The transmission coefficient and the electric field profile magnitudes for a pair of harmonics (n_1 and n_2) oscillating at the same frequency ($|\omega_0 - n_1\Omega| = |\omega_0 - n_2\Omega|$) are the same, namely, $|E_{n_1}^t| = |E_{n_2}^t|$ and $|E_{n_1}^s(y)| = |E_{n_2}^s(y)|$. Independently of the excitation frequency ω_0 (odd multiples of $\Omega/2$), the dominant spectral components of the reflected and transmitted fields oscillate with frequency $|\omega_0 - n\Omega| = \Omega/2$. Further, as the excitation frequency ω_0 increases, the magnitudes of the generated fields decrease, their parity being conserved. As the modulation strength $\Delta\epsilon$ increases, higher-order harmonics become more appreciable and a larger number of wave vectors k_p contribute significantly to the total electric field inside the slab.

The implementation of dynamic metamaterials could provide suitable experimental conditions for detecting such resonances.

ACKNOWLEDGMENTS

P.H. wishes to thank Professor Ari Sihvola for his support and hospitality during a summer stay at the Helsinki University of Technology. He also acknowledges support through the CONACyT Project No. 79180.

APPENDIX: NUMERICAL ANALYSIS NEAR A RESONANCE

Herein, we analyze meticulously the precision of the numerical algorithms near a resonance. This precision depends on the machine ϵ. This analysis leads us to conclude that the resonances are legitimate.

As we pointed out in Sec. IV B, the linear system Eqs. (6)–(9) is solved by using the single-value decomposition method.

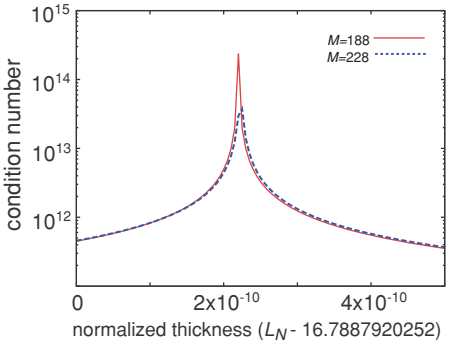

FIG. 7. (Color online) The condition number of $\mathbb{A}$ for orders $M = 188$ and 228, $\Delta\epsilon = 3.4$ (strong modulation) and $\omega_o = \Omega/2$.

For a square matrix $\mathbb{A}$ of coefficients of order M, the parameters

$$\sigma_1 \geqslant \sigma_2 \geqslant \cdots \geqslant \sigma_M \geqslant 0,$$

denominated singular values, are extracted by this method. The condition number of $\mathbb{A}$ can be estimated as

$$\mathrm{cnd}\,(\mathbb{A}) = \sigma_1/\sigma_M. \tag{A1}$$

In principle, the matrix $\mathbb{A}$ is singular if $\mathrm{cnd}(\mathbb{A}) \to \infty$. The error of the calculated σ_i from the true $\hat{\sigma}_i$ is [9]

$$|\sigma_i - \hat{\sigma}_i| < b, \qquad i = 1, \ldots, M \tag{A2}$$

where $b \approx \sigma_1 \epsilon_m$ (ϵ_m being the machine ϵ).

We consider the same resonance discussed in Sec. IV B, that is, $\Delta\epsilon = 3.4$ (strong modulation), $\omega_0 = \Omega/2$, and $a < L_N < a + 5 \times 10^{-10}$ ($a = 16.788\,792\,025\,2$). In Fig. 7, we depict the condition number of the matrix $\mathrm{cnd}(\mathbb{A})$ as a function of the normalized thickness L_N for $M = 188$ and 228. We notice that, apart from roughly two orders of magnitude difference, the plots of D_1/E_0 (Fig. 3) and $\mathrm{cnd}\,(\mathbb{A})$ (Fig. 7) look similar. Consequently, the heights of the peaks of Fig. 3 seem to be proportional to σ_1/σ_M at the resonant thickness. It happens that the σ_i are almost constant in the vicinity of the resonance with the *exception* of σ_M, which varies significantly in this very small interval of L_N. The value of σ_M can be inferred from Fig. 7 by using Eq. (A1) and the fact that $\sigma_1 \approx 11.274$ ($\sigma_1 \approx 11.603$) for $M = 188$ ($M = 228$). Then we obtain that $\min(\sigma_M) \approx 4.75 \times 10^{-14}$ [$\min(\sigma_M) \approx 3.08 \times 10^{-13}$] for $M = 188$ [$M = 228$]. On the other hand, our machine ϵ is $\epsilon_m = 2.2 \times 10^{-16}$; thus the error bound is $b \approx 2.48 \times 10^{-15}$ ($b \approx 2.55 \times 10^{-15}$) for $M = 188$ ($M = 228$). Also, the error bound b is related to the bound for the minimum σ_M that can be obtained *numerically*, that is, $\sigma_M > b$. Therefore, the facts that the variation of σ_M is huge in this small interval and that $\min(\sigma_M)$ nearly reaches the bound b indicate the existence of a legitimate resonance.

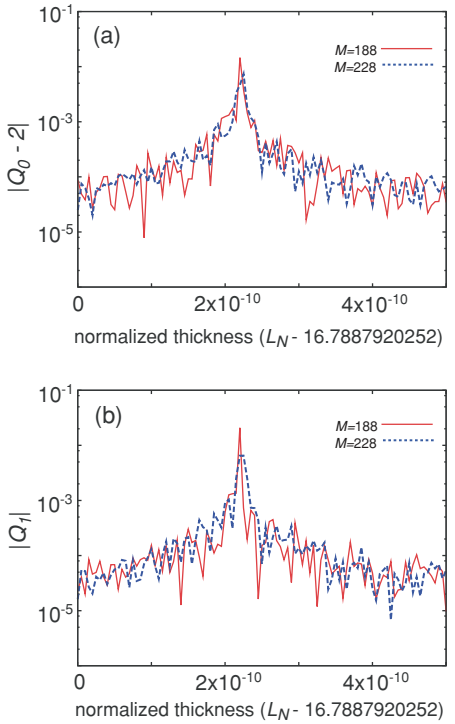

FIG. 8. (Color online) Numerical check near a resonance for $\Delta\epsilon = 3.4$ (strong modulation), $\omega_0 = \Omega/2$, and matrix order $M = 188$ and 228. (a) $|Q_0 - 2|$ as a function of the normalized thickness L_N. (b) $|Q_1|$ as a function of the normalized thickness L_N.

The addition of Eqs. (6) and (7) yields

$$Q_n - 2\delta_{n0} = 0, \tag{A3}$$

where

$$Q_n \equiv \sum_p e_{pn}(\omega_0)\left[\frac{A_p}{E_0}\left(1 + \frac{k_p(\omega_0)c}{\omega_0 - n\Omega}\right) + \frac{B_p}{E_0}\left(1 - \frac{k_p(\omega_0)c}{\omega_0 - n\Omega}\right)\right]. \tag{A4}$$

As an additional check of our numerical solution, we calculate Q_n by using the numerical outcomes for $M = 188$ and 288. Figure 8 shows the plots of $|Q_0 - 2|$ and $|Q_1|$ as functions of the normalized thickness L_N. Thus, these plots show how much the numerical calculations of $|Q_0 - 2|$ and $|Q_1|$ deviate from zero (the exact solution). We mention that the series Q_n converges numerically when $p \approx 17$. The ripple appearing in Fig. 8 is due to the error propagation arising from the sum of large numbers. Also, the amplitude of this ripple is smaller for $M = 228$ than for $M = 188$ (see Fig. 8). The significant-digit number accuracy depends on the condition number of the matrix $\mathbb{A}$. As seen in Figs. 7 and 8, there is a correlation between the deviation from zero and $\mathrm{cnd}\,(\mathbb{A})$.

[1] J. R. Zurita-Sánchez, P. Halevi, and J. C. Cervantes-González, Phys. Rev. A **79**, 053821 (2009).
[2] J. C. Simon, IEEE Trans. Microwave Theory Tech. **8**, 18 (1960).
[3] D. E. Holberg and K. S. Kunz, IEEE Trans. Antennas Propag. **14**, 183 (1966).
[4] C. K. Law, Phys. Rev. A **49**, 433 (1994).
[5] N. V. Budko, Phys. Rev. A **80**, 053817 (2009).

[6] P. Dong, S. F. Preble, J. T. Robinson, S. Manipatruni, and M. Lipson, Phys. Rev. Lett. **100**, 033904 (2008).
[7] A. Khorshidahmad and A. G. Kirk, Opt. Lett. **34**, 3035 (2009).
[8] J. A. Richards, *Analysis of Periodically Time-varying Systems* (Springer-Verlag, Berlin, 1983).
[9] E. Anderson, Z. Bai, C. Bischof, S. Blackford, J. Demmel, J. Dongarra, J. Du Croz, A. Greenbaum, S. Hammarling, A. McKenney, and D. Sorensen, *LAPACK Users' Guide*, 3rd ed. (Society for Industrial and Applied Mathematics, Philadelphia, 1999).